JACS
JOURNAL OF THE AMERICAN CHEMICAL SOCIETY

Article

pubs.acs.org/JACS

Open Access on 08/12/2015

Programmable Nanoscaffolds That Control Ligand Display to a G-Protein-Coupled Receptor in Membranes To Allow Dissection of Multivalent Effects

Andrew V. Dix,[†] Steven M. Moss,[†] Khai Phan,[†] Travis Hoppe,[‡] Silvia Paoletta,[†] Eszter Kozma,[†] Zhan-Guo Gao,[†] Stewart R. Durell,[§] Kenneth A. Jacobson,[†] and Daniel H. Appella*[,†]

[†]Laboratory of Bioorganic Chemistry, NIDDK, [‡]Laboratory of Biochemistry and Genetics, NIDDK, and [§]Laboratory of Cell Biology, CCR, NCI, National Institutes of Health, Bethesda, Maryland 20892, United States

Supporting Information

ABSTRACT: A programmable ligand display system can be used to dissect the multivalent effects of ligand binding to a membrane receptor. An antagonist of the A_{2A} adenosine receptor, a G-protein-coupled receptor that is a drug target for neurodegenerative conditions, was displayed in 35 different multivalent configurations, and binding to A_{2A} was determined. A theoretical model based on statistical mechanics was developed to interpret the binding data, suggesting the importance of receptor dimers. Using this model, extended multivalent arrangements of ligands were constructed with progressive improvements in binding to A_{2A}. The results highlight the ability to use a highly controllable multivalent approach to determine optimal ligand valency and spacing that can be subsequently optimized for binding to a membrane receptor. Models explaining the multivalent binding data are also presented.

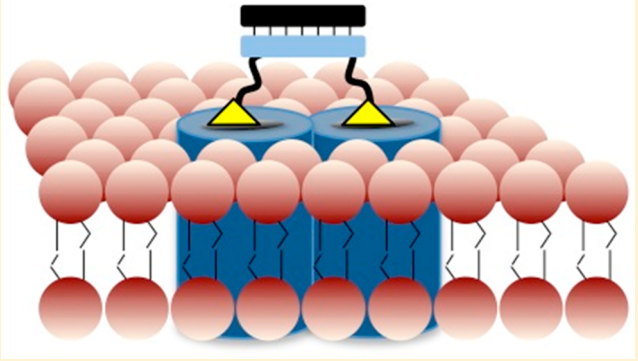

INTRODUCTION

Many crucial biological functions such as cell attachment, growth, and intracellular communications depend on multiple, simultaneous interactions that occur between ligands and receptors at the surfaces of cells.[1,2] The term multivalency describes these binding events, when two or more ligands interact with multiple binding sites of receptors. There has been an intense effort to understand the role of multivalency in the group of receptors known as G-protein-coupled receptors (GPCRs).[3] These receptors are present on the surfaces of all mammalian cells and are responsible for communicating biochemical signals from the exterior environment to a cell's internal machinery. While each GPCR will individually bind to a single molecule of a ligand, such as a hormone or neurotransmitter, the complexity of cellular signaling that results from ligand−receptor binding is the result of numerous additional interactions between GPCRs and other proteins. Collectively, GPCRs regulate a very broad range of physiological responses (such as vision, olfaction, and behavior) as well as the maintenance of key biological systems (such as autonomic nervous, musculoskeletal, cardiovascular, and immune systems).[4] Dysregulation of these receptors is associated with numerous diseases and has spurred the development of small molecule drugs that target GPCRs.[5]

An emerging concept concerning GPCRs is that they interact with each other via a network of protein−protein interactions within a cell's membrane, and there is therefore a need to develop new techniques and approaches to study this network. A deeper understanding of how multivalency controls ligand−GPCR interactions could help to elucidate how these proteins communicate and ultimately provide a means to coordinate GPCR signaling for the treatment of associated human diseases. Based on extensive studies of GPCRs in which fluorescent labeling of either the receptor or ligand is used, there is general agreement that labeled GPCRs can dimerize in the membrane.[6−12] There is additional evidence that higher-order GPCR complexes with at least three labeled proteins can be present.[13] If GPCRs associate within the membrane, then close examination of the multivalent display of ligands for these receptors should provide a complementary approach to study their associations. Identifying a suitable chemical scaffold for the multivalent display of GPCR ligands is challenging. Current chemical scaffolds to examine multivalent effects of GPCR binding are restricted to display ligands at specific valencies that do not allow broad investigation across a range of valencies. For instance, bivalent chemical probes consisting of two ligands covalently linked together by flexible spacers have been used to validate the formation of GPCR dimers and were also used as molecular rulers to approximate adjacent binding site

Received: May 5, 2014
Published: August 12, 2014

dx.doi.org/10.1021/ja504288s | J. Am. Chem. Soc. 2014, 136, 12296−12303

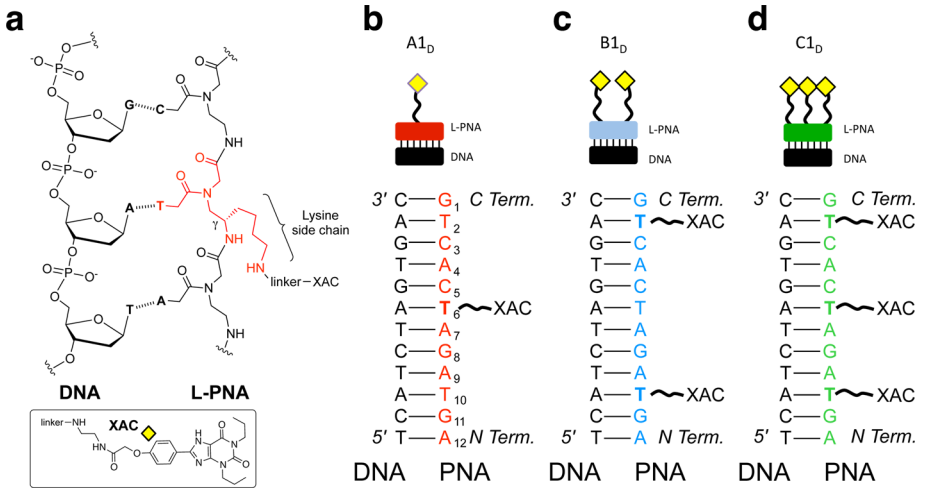

Figure 1. Ligand-modified PNAs. (a) Representation of a L-PNA:DNA duplex as a chemical structure with the γ-lysine side chain modification highlighted in red. XAC is connected to the side chain by two mini-PEG (Boc-8-amino-3,6-dioxaoctanoic acid) linkers. (b–d) L-PNA 12-base oligomer bound to complementary DNA with one XAC ligand (b), two XAC ligands (c), and three XAC ligands per L-PNA (d).

distances.[14−17] Beyond a valency of two ligands, however, it is challenging to generate and study multivalent libraries. Only Jacobson and colleagues have probed higher ligand valencies for adenosine receptors (ARs), where 4−500 ligands were attached to a handful of dendrimers and nanoparticles.[18−20] While multivalent effects were clearly present at high ligand valencies, the heterogeneous nature of these scaffolds prevented an accurate quantification of ligands and limited the in-depth analysis of ligand−receptor interactions. There are several other chemical strategies that have been developed for the multivalent display of ligands on synthetic scaffolds, especially in the area of glycobiology.[1,21−27] However, these existing approaches all have restrictive ranges of valencies or the heterogeneity of a material that limits their usefulness to conduct detailed studies of GPCRs. To thoroughly investigate how ligand multivalency can influence GPCR activity, a new scaffold is needed that would allow more control than what is available in the current molecular toolset.

Recently, we described a new multivalent scaffold that is both highly programmable and exceedingly versatile.[28,29] Using ligand-modified peptide nucleic acids (L-PNAs) in conjunction with a series of complementary DNAs, multivalent libraries can be readily generated that fully control ligand location, spacing, and precise valencies (Figures 1 and 2). In this study, we utilize this systematic multivalent approach to interrogate the A_{2A} adenosine receptor (A_{2A}AR), a GPCR that is a drug target for Parkinson's disease and other neurodegenerative conditions.[30] Structure−activity relationships of ligands that bind to A_{2A}AR are well-known and supported by X-ray crystal structures of the ligand-bound receptor.[31−33] Using our L-PNA approach, multivalent libraries bearing an antagonist of the receptor were generated. These libraries map a broad spectrum of ligand−protein binding associations over multiple ligand valencies and spatial orientations. Binding data for each member of the library was obtained using an established radioligand competition assay, and therefore, fluorescent labeling of protein or ligand was not necessary.[19] Analyses of the multivalent landscapes clearly reveal specific regions of enhanced binding as the numbers of ligands increase, but they also reveal important limitations where more ligands do not improve binding. In addition, the data demonstrate that there is an important spatial component of ligand presentation that allows multivalent effects

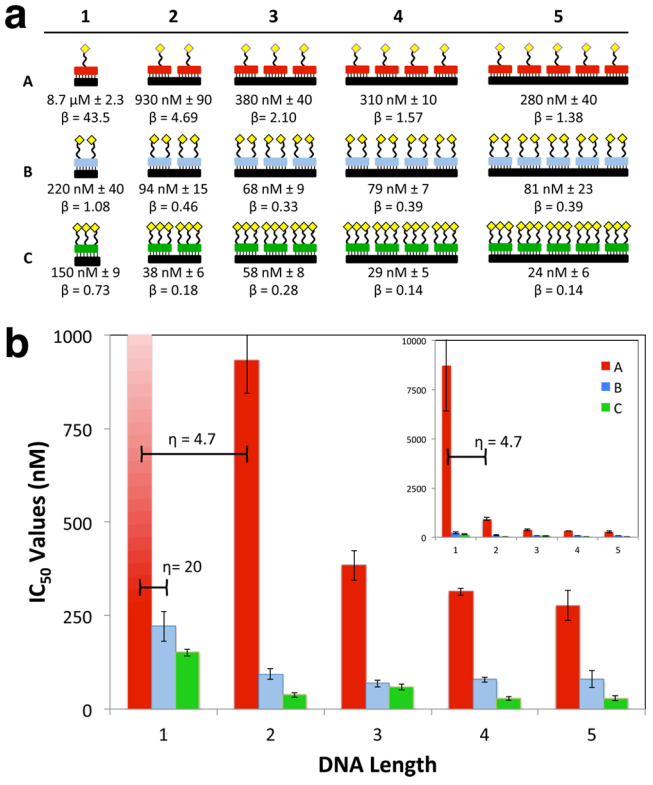

Figure 2. L-PNA:DNA multivalent library and landscape. (a) L-PNA:DNA multivalent library with the associated IC_{50} and β values for binding to A_{2A}AR. (b) Multivalent landscape highlighting the relationships between the A (red), B (blue), and C (green) type L-PNA constructs when annealed to various lengths of DNA. The inset shows the data in full scale, whereas the main window is an enhanced view that enables the observation of more subtle changes in the data. Key η values signal an increase in the individual ligand binding affinity.

to be closely examined. In conjunction with a theoretical model specifically developed to interpret the experimental data, the presence and abundance of A_{2A}AR homodimers within the membrane is suggested. With a deeper understanding of which L-PNAs bind to A_{2A}AR homodimers, sequential attachment of these L-PNA units to each other afforded progressive improve-

dx.doi.org/10.1021/ja504288s | J. Am. Chem. Soc. 2014, 136, 12296−12303

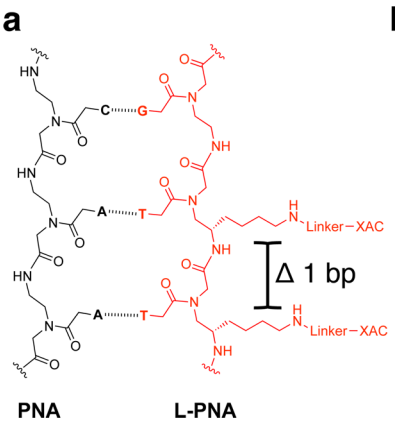

b

Name	L-PNA:PNA	IC_{50} (nM)	Δ bp	η
$A1_P$		1075 ± 170	-	-
$B_{2,3}1_P$		324 ± 36	1	1.6
$B_{6,10}1_P$		216 ± 19	4	2.5
$B_{2,10}1_P$		238 ± 15	8	2.5
$B_{1,14}1_P$		330 ± 46	13	1.6

Figure 3. Bivalent L-PNA:PNA. (a) Representation of a bivalent L-PNA:PNA duplex as a chemical structure. The highlighted L-PNA (red) contains two adjacent ligand-bearing side chains with a spacing of one base pair (bp), which is approximately 3.7 Å. (b) Several bivalent L-PNA:PNAs were generated to determine the affects of axial spacing on receptor binding ability. Along with the monovalent $\mathbf{A1_P}$ control, the four bivalent complexes are summarized including their IC_{50} values in human A_{2A} radioligand binding, the change in axial distance between the ligand side chains, and the η value of the complex compared to $\mathbf{A1_P}$.

ments in binding affinity to the receptor protein. In our optimal multivalent construct, eight antagonist ligands with the proper spacing and orientation on a L-PNA scaffold bind with very high affinity and good selectivity to A_{2A}AR. To explain these data, we propose that A_{2A}AR must be arranged in a higher-order oligomeric state beyond a simple dimer when bound to the multivalent assembly. Our results demonstrate that multivalent libraries based on L-PNA assemblies can be used to study GPCRs and reveal for the first time that specific multivalent arrangements of ligands interact preferentially with A_{2A}AR over other highly similar ligand arrangements.

RESULTS AND DISCUSSION

Initial Library and Multivalent Landscape. To generate a multivalent library of ligand-modified PNA conjugates, a high-affinity AR antagonist, xanthine amine congener (XAC), was conjugated to PNA oligomers via a γ-side chain derived from lysine (γ-Lys, Figure 1a). Ligands attached to this side chain within an L-PNA oligomer do not interfere with the ability of the L-PNA to bind to complementary DNA sequences by traditional Watson−Crick base pairing.[34,35] A series of PNA oligomers, each consisting of 12 nucleobases, was synthesized in which one, two, or three γ-Lys side chains were incorporated into the sequence (Figure 1b−d). The primary amines at the ends of the γ-Lys side chains serve as the attachment points for the XAC ligands. Two mini-PEG (8-amino-3,6-dioxaoctanoic acid) linkers inserted between the amine and the XAC minimize steric repulsion with the receptor protein (Figures S1−S6 and Chart S1 in the Supporting Information). Three L-PNAs were generated in this manner, each containing one, two, or three XAC ligands, referred to as types **A**, **B**, and **C**, respectively (Figure 1b−d). Annealing each L-PNA to complementary DNA sequences designed to bind one to five L-PNAs generates a library of multivalent L-PNA:DNA duplexes (Figure 2a and video S1 in the Supporting Information). Overall, 15 complexes were generated (three different PNAs complexed to five different DNAs) to systematically span a ligand valency between 1 and 15 XAC ligands. Each L-PNA:DNA complex is named according to its individual components. For example, a type **A** construct bearing three L-PNA units along the DNA backbone is referred to as $\mathbf{A3_D}$, which contains three ligands and where the subscript D denotes the DNA backbone (Figure 2a).

Each member of the library was tested for binding affinity using an established human A_{2A}AR membrane-based radioligand inhibition assay to explore the effects on protein binding of increasing the ligand valency and density.[19] Although such protocols have become standard in the investigation of GPCR behavior, membrane binding assay data can be complicated by the presence of multiple receptor binding states.[36−38] These binding isotherms are a composite of these states, and special cases can highlight multiple binding thresholds (i.e., IC_{50} or K_i values). However, they are typically observed as a monophasic binding isotherm. In our experiments, only monophasic isotherms were observed, which provide a single binding affinity for each compound. These affinities are presented in Figure 2a and in the multivalent landscape plotted in Figure 2b. Each construct was measured in triplicate over seven different concentrations. To confirm these findings, select compounds were examined using a recently reported whole-cell assay of receptor binding by flow cytometry adapted to the A_{2A}R.[39] The results from binding in membranes and whole cells were equivalent (Chart S2 in the Supporting Information). Non-specific binding effects[26] were examined using an acetylated form of the type **C** PNA (Ac-**C**) that lacks any XAC ligand (Figure S19 in the Supporting Information). There was no nonspecific binding observed with the complex $\mathbf{AcC1_D}$ (Chart S6 in the Supporting Information).

One way to analyze data from a multivalent screen is to calculate the β-parameter for each member of the library [$\beta = K_d$(L-PNA:DNA)/K_d (monomeric ligand)].[40] As initially established by Whitesides and colleagues, β describes the benefit of the multivalent scaffold relative to the monovalent ligand, and lower values signal enhanced binding due to multivalent effects. For each member of the multivalent library, we calculated the β values shown below the IC_{50} values in Figure 2a. These values reveal some important features. The attachment of one ligand to the L-PNA:DNA ($\mathbf{A1_D}$) scaffold lowers the binding affinity compared to the ligand alone, an expected decrease due to the large molecular weight of the ligand plus scaffold complex (7980 Da) compared to the ligand alone (428 Da). Furthermore, adding mini-PEG linkers to XAC lowers the binding affinity. Similar results have been observed in the work of Jacobson using the same ligand on dendrimers and gold nanoparticles.[18−20] The addition of more ligands to the scaffold

dx.doi.org/10.1021/ja504288s | J. Am. Chem. Soc. 2014, 136, 12296−12303

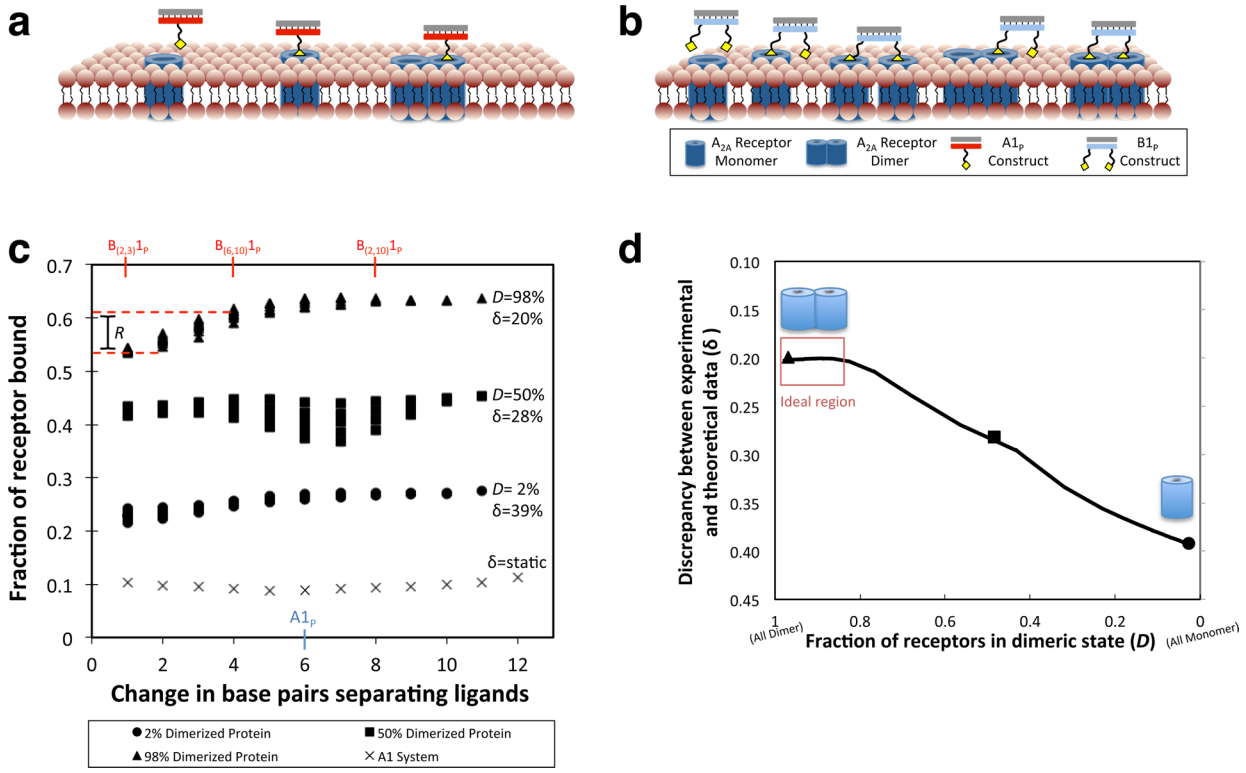

Figure 4. Statistical model. The model assumes that only a discrete number of different binding states exist between L-PNA:PNA and the receptor. A subset of these states is highlighted for the (a) monovalent complex and (b) bivalent complexes. (c) When every possible ligand configuration of $\mathbf{A1_P}$ and $\mathbf{B1_P}$ complexes was used, the model samples an ensemble of states in accordance with a specific fraction of protein in the dimeric state. (d) This information can then be extrapolated and plotted as the fraction of receptors in the dimeric state (D) versus the discrepancy (δ) between the theoretical and experimentally observed data.

quickly overcomes any loss in binding. This observation signals a multivalent effect. While the β values identify the most potent binders in the library, the patterns of improvements in affinity over the entire data set indicated that different types of multivalent effects occur as the number of ligands increases.

Therefore, a new method was developed to analyze the results from the multivalent screen. We define the parameter η as the change in binding affinity between any two adjacent L-PNA:DNA complexes in Figure 2a when the change in ligand valency is normalized. When comparing two complexes, η values of approximately 1 indicate that individual ligand binding affinity is roughly the same and that any improvements in binding are due solely to the integral increase in the number of ligands. Values of η greater than 2 suggest a statistically significant increase in the individual ligand binding affinity that exceeds the expected improvement from simply having more ligands. When examined in this manner the multivalent landscape in Figure 2b indicates that most η values are near 1 (Charts S7 and S8 in the Supporting Information). However, η values greatly exceed 1 when comparing $\mathbf{A1_D}$ to either $\mathbf{A2_D}$ (η = 4.7, p = 0.016) or $\mathbf{B1_D}$ (η = 19.8, p = 0.012), and these results indicate that the two ligands of $\mathbf{A2_D}$ and $\mathbf{B1_D}$ simultaneously bind to two A_{2A}AR proteins. The main conclusion from this analysis of the multivalent landscape is that the most significant improvements in ligand−receptor binding occur when moving from a valency of 1 to 2 ligands.

Ligand-Spacing Study. Our initial results indicate that a L-PNA:DNA complex bearing two XAC ligands binds significantly better than a corresponding monovalent complex. Next, we explored the effects of ligand spacing. A series of bivalent constructs were examined where the two γ-Lys side chains bearing XAC ligands were systematically shifted along the PNA backbone (Figure 3 and Figures S7−S12 in the Supporting Information). To minimize the electrostatic influence of the negative charges on the DNA phosphodiester backbone, the DNA was replaced with a PNA that was complementary in sequence (Figures S13−S15 in the Supporting Information). Constructs prepared in this manner bear a P subscript. It is well-established that PNA:PNA duplexes maintain traditional nucleobase pairings in double-helical structures.[34] Experimental results revealed that DNA can have a *negative effect* on binding because $\mathbf{A1_P}$ was 8-fold more potent than $\mathbf{A1_D}$ (p = 0.0015). With the exception of lysine residues added at the termini to promote aqueous solubility, the resulting L-PNA:PNA duplex is charge-neutral and should not experience charge−charge repulsion with phosphate groups on the membrane containing the receptor. In total, four $\mathbf{B1_P}$ complexes were generated ($\mathbf{B_{2,3}1_P}$, $\mathbf{B_{6,10}1_P}$, $\mathbf{B_{2,10}1_P}$, and $\mathbf{B_{1,14}1_P}$) with various distances between the ligands, where the side chains on the L-PNA backbone were separated by 1, 4, 8, or 13 nucleobases (Figure 3a).

The bivalent L-PNA:PNA complexes all bound with higher affinity to A_{2A}AR (η = 1.6−2.5, $p \geq 0.007$) compared to $\mathbf{A1_P}$ (Figure 3b). Within the series of bivalent constructs, the narrowest ($\mathbf{B_{2,3}1_P}$) and the widest ($\mathbf{B_{1,14}1_P}$) complexes were the weakest binders. The $\mathbf{B_{6,10}1_P}$ and $\mathbf{B_{2,10}1_P}$ complexes bound with higher affinities yet were experimentally indistinguishable from each other at this level ($p \geq 0.05$). Although less dramatic compared to the previous multivalent screen, the binding data and η values indicate that the strength of ligand binding in this

dx.doi.org/10.1021/ja504288s | J. Am. Chem. Soc. 2014, 136, 12296−12303

series of bivalent complexes depends on the distance and angle between the side chains that display the ligands.

Theoretical Model and Docking. Based on the data from the multivalent screens, it seemed likely that bivalent complexes bind to homodimeric pairs of A_{2A} receptors. To investigate this possibility in more detail, we developed a coarse-grained statistical mechanics model to interpret the experimental binding data in Figure 3b and suggested the relative abundance of dimeric versus monomeric receptors (a full description of the model is presented in the Supporting Information). The model examines the relative ability of all 78 possible configurations of monovalent (12) and bivalent (66) side chain combinations along the L-PNA:PNA backbone to bind to a theoretical receptor (video S2 in the Supporting Information shows the set of bivalent side chains). The linker groups attached to the side chains of the ligands are flexible, thus the conformational states accessible to each side chain were modeled as a polymer with a self-avoiding walk. The receptors were modeled as two concentric circles, an outer circle representing the excluded volume portion of the receptor and an inner circle representing its ligand binding site. Ensembles of different receptor densities were placed in a two-dimensional plane representing the lipid bilayer of a membrane. Discrete ratios of receptor dimers and monomers were assigned, ranging from all monomers to all dimers. Each side chain configuration of the L-PNA:PNA construct was examined for its binding potential to the receptor ensemble.

By assigning a fixed energy to each interaction, only a discrete number of different binding states exist between L-PNA:PNA and the receptor. Examples of these states for the monovalent ($\mathbf{A_{1P}}$) and bivalent ($\mathbf{B_{1P}}$) complexes are highlighted in Figure 4a,b. In this model, the enthalpy of ligand binding to the receptor was assumed to be the same for each state in which there is a binding event. Therefore, only the changes in entropy of receptor binding between the different L-PNA:PNAs were considered in the subsequent calculations. The model determines the probability of occurrence for each possible state, calculates the density of states for each protein ensemble, and subsequently provides a partition function with an energetic term (based on the entropy of binding) that represents the likelihood of receptor dimerization. Finally, the fraction of ligand-bound receptors in the ensembles is calculated for each L-PNA:PNA configuration. In Figure 4c, some of these data are presented for four different data sets. Each data set in the figure (▲, ■, ●) consists of the 66 different combinations of L-PNA:PNA bivalent complexes interacting with receptors at a discrete ratio of dimer to monomer (D). The × represents the 12 possible monovalent L-PNA:PNAs interacting with the receptors.

Depending on the percentage of receptor dimer (D) assigned in the model, there are clear differences in the predicted binding of bivalent L-PNA:PNAs. For instance, when only 2% of receptors exist as dimers (D = 2%), there is a low fraction of bound receptors across the set of 66 possible bivalent L-PNA:PNAs (●). If 98% of receptors are dimers (D = 98%), the predicted fraction of bound receptors is much higher (▲). These differences exist for bivalent L-PNA:PNA. For the 12 possible monovalent L-PNA:PNAs (×), there is no change in the fraction of bound receptors as the percentage of dimer increases because the single ligand binds equally to all states of the receptor regardless of whether it is a dimer or monomer.

The experimental data were compared with the theoretical model to estimate the percentage of receptor dimers. The red bars at the top of Figure 4c show where the experimental bivalent L-PNA:PNAs from Figure 3b align within the model's 66 possible L-PNA:PNA configurations. The next goal was to determine which data set (▲, ■, ●, or others) had the best fit with the experimental values. To make this evaluation, ratios of IC_{50} values, represented by R, from Figure 3b are directly compared to the R ratios for the same L-PNA:PNA complexes in the model. This was necessary to compare the theoretical model with the experimental data. An example of this ratio is shown in Figure 4c, which is the R ratio of IC_{50} values for $\mathbf{B_{2,3}1_P}$ to $\mathbf{B_{6,10}1_P}$. The R from experimental data is compared to the same ratio predicted by the model in each data set (for more detail on determining the R values, see eqs 11 and 12 in the theoretical model in Supporting Information). In total, there are six experimentally determined R ratios derived from Figure 3 that are compared to the analogous ratios in the different data sets of the model. Discrepancies between the experimental and theoretical values are designated by delta (δ). The magnitude of the discrepancy between experiment and theory was used as a guide to assign the most likely percentage of receptor dimer (Figure 4d).

The analysis suggests that bivalent L-PNA:PNA binds to A_{2A} receptors that exist as dimers. A model where the receptors exist largely as monomers does not account for the observed experimental data ($\delta \geq 40\%$). The best overlap between the experimental and theoretical data, signified by the smallest δ value, is in the realm of 80−95% of receptors existing as dimers (see "ideal region" in Figure 4d) and the remaining portion as monomers ($\delta \leq 20\%$).

A molecular model further demonstrates that a bivalent L-PNA:PNA could bind to a dimer of A_{2A} proteins without excessive strain or clear steric clashing between the scaffold and the proteins. A dimeric A_{2A}AR was built and modeled to interact with $\mathbf{B_{6,10}1_P}$ (Figure 5a). The structure of the A_{2A}AR monomers

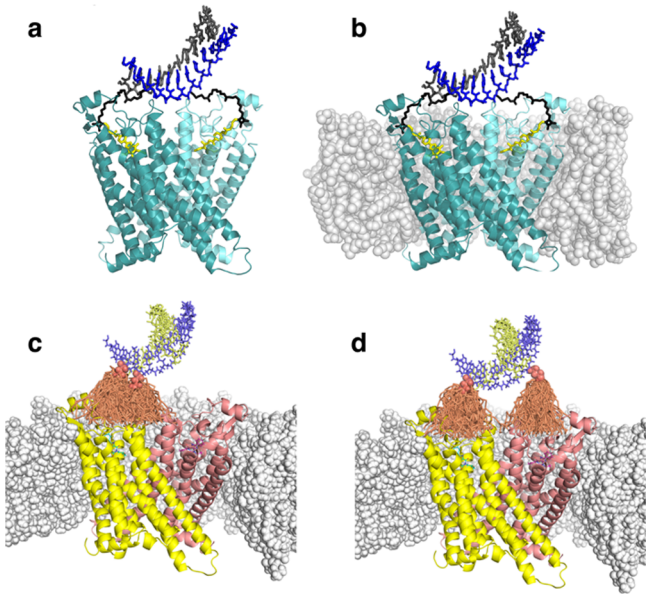

Figure 5. Molecular modeling. A molecular model of a proposed A_{2A} dimer was built based on a known antagonist-bound crystal structure of the monomer. The $\mathbf{B_{(6,10)}1_P}$ complex was modeled with the dimer, both (a) without and (b) with the phospholipid bilayer (cellular membrane). When a subset of the data from the statistical model was used, possible side chain organizations are superimposed on the model for the (c) $\mathbf{B_{(2,3)}1_P}$ and (d) $\mathbf{B_{(6,10)}1_P}$ complexes.

dx.doi.org/10.1021/ja504288s | J. Am. Chem. Soc. 2014, 136, 12296−12303

was modeled on high-resolution X-ray crystal structures (PDB IDs: 3REY and 4EIY).[31,41] The likely contact regions between the protomers were determined through protein−protein docking and data from model systems.[42] A PNA:PNA duplex model was created wherein the helical conformations were derived from the NMR solution structure of a γ-methylated PNA duplex 8-mer (PDB accession code 2KVJ).[43] The duplex model was then connected to the bound XAC ligand through mini-PEG linkers that are identical to the ones used in the multivalent libraries. The construct was then optimized to an energy minimum and is displayed without (Figure 5a) and with (Figure 5b) the membrane. Both the molecular and statistical models suggest that the linkers are sufficient in length to allow access to both binding sites with an optimal side chain placement. Additionally, the duplex backbone has ample space to hover over the protein surface without steric repulsion. These models represent a static snapshot of binding. A clearer representation of the flexibility associated with the side chains is shown in Figure 5c,d. Models of the proposed A_{2A}AR dimer are overlaid with two bivalent L-PNA:PNA complexes. A subset of the side chain conformations from the statistical model is displayed. As seen in Figure 5c, the side chains of $\mathbf{B}_{2,3}\mathbf{1}_P$ do not overlap very well to simultaneously interact with both binding sites of the proposed A_{2A}AR dimer. In $\mathbf{B}_{6,10}\mathbf{1}_P$ (Figure 5d), the side chains are more favorably arranged to simultaneously bind the dimer. This matches our experimental data; $\mathbf{B}_{6,10}\mathbf{1}_P$ binds with slightly higher affinity to A_{2A}AR than $\mathbf{B}_{2,3}\mathbf{1}_P$ (IC_{50} values of 210 nM versus 320 nM, Figure 3b).

To further test the structural feasibility of the A_{2A}AR homodimer/$\mathbf{B}_{(6,10)}\mathbf{1}_P$ complex, the stability was tested by molecular dynamics computer simulations. To account for the heterogeneous environment, the system included explicit lipid molecules for the membrane bilayer and explicit water molecules for the solvent. The stability of the protein and PNA components is depicted by the time course of the root mean square deviations (rmsd) (Figure S21 in the Supporting Information). The deviations are from the coordinates obtained at 1.0 ns of production dynamics, allowing for equilibration under the constant pressure and temperature constraints. As seen by the leveling-off of the curves, net changes in both the protein and PNA structures finish at approximately 500.0 ps. For the A_{2A}AR protein, the similar rmsd magnitudes for the dimer and the two monomers separately indicate that the monomers are not moving apart or changing relative orientation over time. The results for the PNA duplex indicate slightly greater stability for the base pairs compared to the backbone, as described by Autiero et al. for a different sequence of PNA.[44] Likewise, similar magnitudes of PNA rmsd values, approximately 1.8 Å, are obtained for the two systems. Finally, as portrayed in the movie of the trajectory (video S3 in the Supporting Information), the main change in the conformation of the complex is the moving away of the duplex from the membrane-bound receptor dimer. This allows for greater access of water to the polar elements of the PNA construct and the lipid headgroups of the proximal membrane. However, this drift is restrained by the bound XAC molecules, which maintain their docked positions in the binding sites of the two A_{2A}AR proteins.

L-PNA:PNA Multivalent Landscape. Comparing results from L-PNA:DNA and L-PNA:PNA demonstrated that the DNA can have a detrimental effect on binding to the receptor at low valencies. Bivalent L-PNA:PNA duplexes were used to examine the effects of intraligand distances on binding to A_{2A}AR. This approach was extended to higher valencies using longer PNAs as a replacement for DNA. Therefore, a modified PNA construct that can be made up to 48 bases in length was developed to support the binding of up to four complementary L-PNAs (with each L-PNA having between one and three side chains bearing a XAC ligand) (Figures S16−S18 in the Supporting Information). These modified PNAs contain an *N*,*N*-dimethyllysine residue after every 12th nucleobase, which allows conformational flexibility between adjacent L-PNAs. A second library containing 16 L-PNA:PNAs was constructed and used to generate a multivalent landscape by determining the binding affinity for each member of the library.

The multivalent library for L-PNA:PNA is shown in Figure 6a, spanning valencies from 1 to 12 XAC ligands. The multivalent effects of two different bivalent type **B** PNAs were also explored in this library. Previously, $\mathbf{B}_{6,10}\mathbf{1}_P$ and $\mathbf{B}_{2,10}\mathbf{1}_P$ showed experimentally indistinguishable binding affinities to A_{2A} when examined as a 1:1 L-PNA:PNA complex (Figure 3b). With a better understanding of the likelihood for A_{2A} receptors to form dimers, we were particularly interested to see if these constructs would show enhanced binding at higher valencies.

The results of screening this new L-PNA:PNA library are presented in Figure 6. Similar to the original multivalent screen, there is a significant enhancement of ligand binding efficiency when comparing valencies of one to two ligands (η = 2.5), and for the most part, all other improvements in binding affinity can be accounted for by the corresponding increase in ligand valency ($\eta \cong 1$, Charts S9 and S10 in the Supporting Information). Additionally, an analysis of the Hill slopes further supported the general trend of enhanced binding properties (Chart S3 in the Supporting Information).

There was no observed nonspecific binding of the control complex $AcC1_P$ in which the PNA Ac-C was complexed with complementary PNA (Figure S19 and Chart S6 in the Supporting Information). Remarkably, there is one data point in the multivalent landscape that is distinctly different: $\mathbf{B}_{6,10}\mathbf{4}_P$ has a binding affinity that is markedly better than any of its surrounding neighbors (β = 0.13). This specific L-PNA:PNA has a valency of eight XAC-bearing side chains, arranged by pairs on four L-PNAs that are bound to a complementary PNA sequence containing 48 bases. The interligand spacing on the bivalent $\mathbf{B}_{6,10}$ PNA should be optimized for binding to an A_{2A} dimeric pair, as shown previously (Figure 3b). A highly similar complex with identical size and valency (namely, $\mathbf{B}_{2,10}\mathbf{4}_P$) binds significantly weaker (3-fold, β = 0.34), as do other L-PNA:PNAs with lower or higher valencies. A closer examination of the data series for $\mathbf{B}_{6,10}$ shows sequential improvement in binding affinity as successive additions of the complementary PNA are incorporated (with regard to IC_{50} values, $\mathbf{B}_{6,10}\mathbf{1}_P > \mathbf{B}_{6,10}\mathbf{2}_P > \mathbf{B}_{6,10}\mathbf{3}_P > \mathbf{B}_{6,10}\mathbf{4}_P$). Interestingly, the same series with $\mathbf{B}_{2,10}$ does not show the same successive improvements in binding to A_{2A}. This divergent trend was also observed in the Hill slope analysis. Further studies with $\mathbf{B}_{6,10}\mathbf{4}_P$ show that it retains physiological antagonist activity in an in vivo cAMP functional assay (Figure S22 in the Supporting Information). Additionally, when compared to its homologues A_1 and A_3, $\mathbf{B}_{6,10}\mathbf{4}_P$ demonstrated enhanced selectivity for A_{2A} receptors that significantly exceeds that of the monovalent XAC ligand (Figure 6a and Chart S4 in the Supporting Information). These results all suggest that $\mathbf{B}_{6,10}\mathbf{4}_P$ has the proper dimensions and interligand spacing to bind simultaneously to multiple dimeric pairs of A_{2A} receptors.

dx.doi.org/10.1021/ja504288s | J. Am. Chem. Soc. 2014, 136, 12296−12303

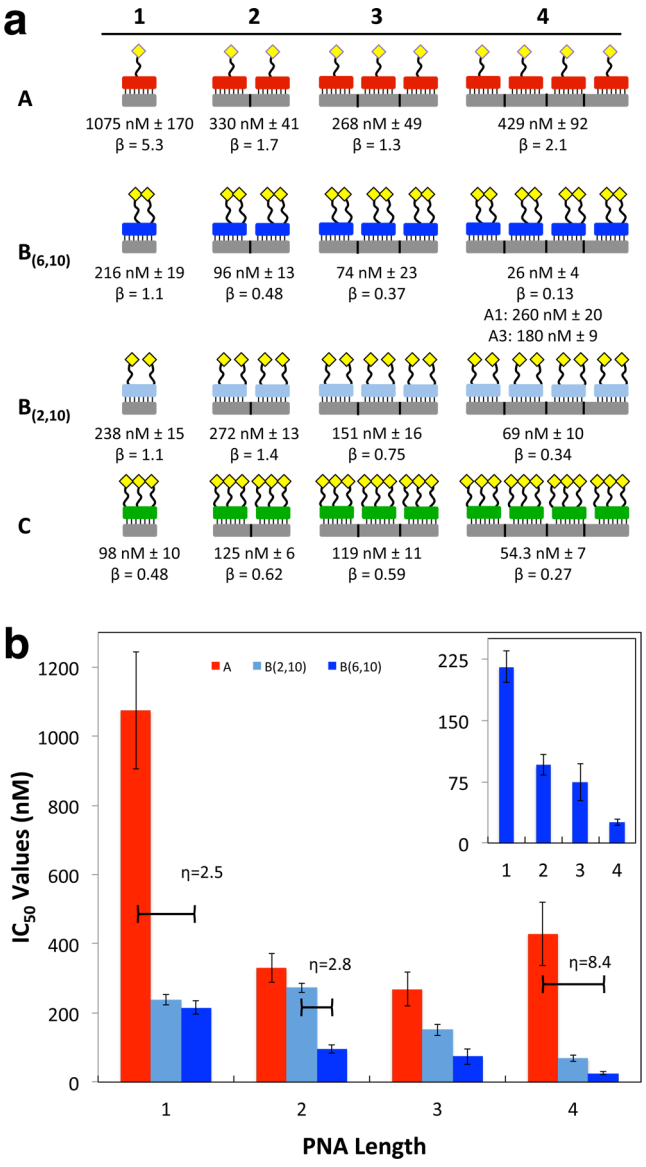

Figure 6. L-PNA:PNA multivalent landscape. (a) L-PNA:PNA multivalent library with the associated IC_{50} and β values. Complex $\mathbf{B}_{(6,10)}\mathbf{4}_P$ was also screened for binding to other human AR subtypes A_1AR (260 nM) and A_3AR (180 nM). Black lines within the gray boxes indicate positions of the *N*,*N*-dimethyllysines. (b) Multivalent landscape highlighting the relationships between the **A** (red), $\mathbf{B}_{(2,10)}$ (light blue), $\mathbf{B}_{(6,10)}$ (dark blue), and **C** (green) type L-PNA constructs when annealed to various lengths of complementary PNA. The inset shows the progressively increasing binding affinity of the $\mathbf{B}_{(6,10)}$ family as the length of the PNA complement is increased. Key η values are noted.

CONCLUSIONS

Programmable multivalent scaffolds that allow ligands to be displayed across a range of valencies and geometries can be used to study receptors at the membrane level. The fundamental investigational tool for this type of scaffold is the ligand-bearing L-PNA that can be assembled onto complementary sequences of DNA or PNA. For this work, a total of 35 different multivalent constructs were synthesized, and each member of this library was tested for binding to the A_{2A} receptor in an established radioligand displacement assay. The binding data were assembled to depict multivalent landscapes that were closely examined (with the help of β and η values) for regions of enhanced binding. Significant improvements in binding affinity were observed when comparing monovalent to bivalent display of the XAC ligand. This prompted a closer examination of the bivalent L-PNAs to determine whether A_{2A} dimer formation is important. For these experiments, the DNA part of the scaffold was replaced with another PNA to minimize electrostatic repulsion. To probe the likelihood of receptor dimers, the interligand distance dependence on binding was examined, and a theoretical model was developed to interpret the experimental data. The model suggests that A_{2A} exists predominantly as a dimer when bivalent L-PNA:PNA binds the receptor and that both XAC ligands can interact simultaneously with the dimer. These results agree with previous studies that suggest the presence of unligated A_{2A} homodimers.[45,46] In addition, recent crystallographic studies have demonstrated that several GPCRs can exist as dimeric species.[47,48]

Previous GPCR research provided evidence that some receptors assemble into higher-order oligomers consisting of three or more proteins. Screening our L-PNA:PNA multivalent library revealed $\mathbf{B}_{6,10}\mathbf{4}_P$ as an exceptional binder compared to highly similar members within the same library. For instance, $\mathbf{A4}_P$, $\mathbf{B}_{6,10}\mathbf{4}_P$, and $\mathbf{C4}_P$ only differ in the number of ligands they display (4, 8, and 12) as they all have the same PNA scaffold (4 L-PNAs bound to a 48-base complementary PNA). Yet $\mathbf{A4}_P$ and $\mathbf{C4}_P$ bind 16 and 2 times more weakly to A_{2A} compared to $\mathbf{B}_{6,10}\mathbf{4}_P$. This difference is not simply related to the change in ligand valency. Even more striking is the comparison between $\mathbf{B}_{6,10}\mathbf{4}_P$ and $\mathbf{B}_{2,10}\mathbf{4}_P$, which differ only in the placement of two XAC ligand side chains yet exhibit a 3-fold difference in binding affinity. We propose that $\mathbf{B}_{6,10}\mathbf{4}_P$ binds to A_{2A} dimers arranged in higher-order oligomeric structures. It is important to note that our results do not show how the receptor associates in the absence of a ligand, and it is possible that $\mathbf{B}_{6,10}\mathbf{4}_P$ drives formation of the proposed higher-order structure. At the same time, X-ray crystallography studies have indicated that dimeric pairs of GPCRs could interact favorably in the packing lattice of the solid state.[47,48] We believe that $\mathbf{B}_{6,10}\mathbf{4}_P$ is the first example of a discrete multivalent pharmacological ligand binding to a higher-order arrangement of GPCRs.

The L-PNA system provides rigorous control over ligand valency and density, which can be reliably programmed into a spatially defined scaffold. The system also synergizes with the development of theoretical models to interpret the data. A key feature of the bivalent L-PNAs is the ability to change side chain spacing on the rigid scaffold without altering the molecular size or number of rotatable bonds. The ability to maintain such consistency within the series of bivalent L-PNA:PNA in Figure 3b while subtly altering the ligand spacing is unique among bivalent pharmacological probes and facilitates the development of theoretical models. Indeed, no other currently available bivalent or multivalent approach can investigate a GPCR system with a similar level of precision or detail. Investigations of other ligand–receptor systems using the L-PNA scaffolds should provide detailed snapshots of different multivalent landscapes that can be used to probe other types of membrane receptors.

ASSOCIATED CONTENT

Supporting Information

Synthetic procedures, characterization data, assay protocols, and supporting data. This material is available free of charge via the Internet at http://pubs.acs.org.

dx.doi.org/10.1021/ja504288s | J. Am. Chem. Soc. 2014, 136, 12296–12303

AUTHOR INFORMATION

Corresponding Author

appellad@niddk.nih.gov

Notes

The authors declare no competing financial interest.

ACKNOWLEDGMENTS

This research was supported by the Intramural Research Program of NIDDK, NIH. We gratefully acknowledge Dr. John Lloyd and the mass spectrometry core facility of NIDDK for analysis of all PNA samples. This study utilized the high-performance computational capabilities of the Biowulf Linux cluster at the National Institutes of Health, Bethesda, MD (http://biowulf.nih.gov). We also thank George Lieman and Lisa Jenkins for review and comments on the manuscript.

REFERENCES

(1) Mammen, M.; Choi, S.; Whitesides, G. M. *Angew. Chem., Int. Ed.* **1998**, *37*, 2754−2794.

(2) Fasting, C.; Schalley, C. A.; Weber, M.; Seitz, O.; Hecht, S.; Koksch, B.; Dernedde, J.; Graf, C.; Knapp, E. W.; Haag, R. *Angew. Chem., Int. Ed.* **2012**, *51*, 10472−10498.

(3) Jacobson, K. A. *Trends Pharmacol. Sci.* **2010**, *31*, 575−579.

(4) Rosenbaum, D. M.; Rasmussen, S. G.; Kobilka, B. K. *Nature* **2009**, *459*, 356−363.

(5) Overington, J. P.; Al-Lazikani, B.; Hopkins, A. L. *Nat. Rev. Drug Discovery* **2006**, *5*, 993−996.

(6) Fanelli, F.; Seeber, M.; Felline, A.; Casciari, D.; Raimondi, F. *Prog. Mol. Biol. Transl. Sci.* **2013**, *117*, 105−142.

(7) Wertman, J.; Dupre, D. J. *J. Recept. Signal Transduction Res.* **2013**, *33*, 135−138.

(8) Teitler, M.; Klein, M. T. *Pharmacol. Ther.* **2012**, *133*, 205−217.

(9) Albizu, L.; Cottet, M.; Kralikova, M.; Stoev, S.; Seyer, R.; Brabet, I.; Roux, T.; Bazin, H.; Bourrier, E.; Lamarque, L.; Breton, C.; Rives, M. L.; Newman, A.; Javitch, J.; Trinquet, E.; Manning, M.; Pin, J. P.; Mouillac, B.; Durroux, T. *Nat. Chem. Biol.* **2010**, *6*, 587−594.

(10) Milligan, G. *Mol. Pharmacol.* **2004**, *66*, 1−7.

(11) Parnot, C.; Kobilka, B. *Nat. Struct. Mol. Biol.* **2004**, *11*, 691−692.

(12) Franco, R.; Martinez-Pinilla, E.; Ricobaraza, A.; McCormick, P. J. *Prog. Mol. Biol. Transl. Sci.* **2013**, *117*, 143−162.

(13) Gandia, J.; Galino, J.; Amaral, O. B.; Soriano, A.; Lluis, C.; Franco, R.; Ciruela, F. *FEBS Lett.* **2008**, *582*, 2979−2984.

(14) Shan, M.; Carlson, K. E.; Bujotzek, A.; Wellner, A.; Gust, R.; Weber, M.; Katzenellenbogen, J. A.; Haag, R. *ACS Chem. Biol.* **2013**, *8*, 707−715.

(15) Shonberg, J.; Scammells, P. J.; Capuano, B. *ChemMedChem* **2011**, *6*, 963−974.

(16) Daniels, D. J.; Lenard, N. R.; Etienne, C. L.; Law, P. Y.; Roerig, S. C.; Portoghese, P. S. *Proc. Natl. Acad. Sci. U.S.A.* **2005**, *102*, 19208−19213.

(17) Portoghese, P. S.; Ronsisvalle, G.; Larson, D. L.; Yim, C. B.; Sayre, L. M.; Takemori, A. E. *Life Sci.* **1982**, *31*, 1283−1286.

(18) Jayasekara, P. S.; Phan, K.; Tosh, D. K.; Kumar, T. S.; Moss, S. M.; Zhang, G.; Barchi, J. J. J.; Gao, Z. G.; Jacobson, K. A. *Purinergic Signalling* **2013**, *9*, 183−198.

(19) Kecskes, A.; Tosh, D. K.; Wei, Q.; Gao, Z. G.; Jacobson, K. A. *Bioconjugate Chem.* **2011**, *22*, 1115−1127.

(20) Keene, A. M.; Balasubramanian, R.; Lloyd, J.; Shainberg, A.; Jacobson, K. A. *Biochem. Pharmacol.* **2010**, *80*, 188−196.

(21) Kiessling, L. L.; Grim, J. C. *Chem. Soc. Rev.* **2013**, *42*, 4476−4491.

(22) Bernardi, A.; Jimenez-Barbero, J.; Casnati, A.; De Castro, C.; Darbre, T.; Fieschi, F.; Finne, J.; Funken, H.; Jaeger, K. E.; Lahmann, M.; Lindhorst, T. K.; Marradi, M.; Messner, P.; Molinaro, A.; Murphy, P. V.; Nativi, C.; Oscarson, S.; Penades, S.; Peri, F.; Pieters, R. J.; Renaudet, O.; Reymond, J. L.; Richichi, B.; Rojo, J.; Sansone, F.; Schaffer, C.; Turnbull, W. B.; Velasco-Torrijos, T.; Vidal, S.; Vincent, S.; Wennekes, T.; Zuilhof, H.; Imberty, A. *Chem. Soc. Rev.* **2013**, *42*, 4709−4727.

(23) Le Naour, M.; Akgun, E.; Yekkirala, A.; Lunzer, M. M.; Powers, M. D.; Kalyuzhny, A. E.; Portoghese, P. S. *J. Med. Chem.* **2013**, *56*, 5505−5513.

(24) Jung, H.; Robison, A. D.; Cremer, P. S. *J. Struct. Biol.* **2009**, *168*, 90−94.

(25) Nelson, A.; Belitsky, J. M.; Vidal, S.; Joiner, C. S.; Baum, L. G.; Stoddart, J. F. *J. Am. Chem. Soc.* **2004**, *126*, 11914−11922.

(26) Zhang, Z.; Merritt, E. A.; Ahn, M.; Roach, C.; Hou, Z.; Verlinde, C. L.; Hol, W. G.; Fan, E. *J. Am. Chem. Soc.* **2002**, *124*, 12991−12998.

(27) Kitov, P. I.; Sadowska, J. M.; Mulvey, G.; Armstrong, G. D.; Ling, H.; Pannu, N. S.; Read, R. J.; Bundle, D. R. *Nature* **2000**, *403*, 669−672.

(28) Englund, E. A.; Wang, D.; Fujigaki, H.; Sakai, H.; Micklitsch, C. M.; Ghirlando, R.; Martin-Manso, G.; Pendrak, M. L.; Roberts, D. D.; Durell, S. R.; Appella, D. H. *Nat. Commun.* **2012**, *3*, 614.

(29) Englund, E. A.; Appella, D. H. *Angew. Chem., Int. Ed.* **2007**, *46*, 1414−1418.

(30) Varani, K.; MacLennan, S.; Granieri, E.; Borea, P. A. *FASEB J.* **2010**, *24*, 587−598.

(31) Dore, A. S.; Robertson, N.; Errey, J. C.; Ng, I.; Hollenstein, K.; Tehan, B.; Hurrell, E.; Bennett, K.; Congreve, M.; Magnani, F.; Tate, C. G.; Weir, M.; Marshall, F. H. *Structure* **2011**, *19*, 1283−1293.

(32) Lebon, G.; Warne, T.; Edwards, P. C.; Bennett, K.; Langmead, C. J.; Leslie, A. G.; Tate, C. G. *Nature* **2011**, *474*, 521−525.

(33) Jacobson, K. A.; Gallo-Rodriguez, C.; Melman, N.; Fischer, B.; Maillard, M.; van Bergen, A.; van Galen, P. J.; Karton, Y. *J. Med. Chem.* **1993**, *36*, 1333−1342.

(34) Wittung, P.; Nielsen, P. E.; Buchardt, O.; Egholm, M.; Norden, B. *Nature* **1994**, *368*, 561−563.

(35) Egholm, M.; Buchardt, O.; Christensen, L.; Behrens, C.; Freier, S. M.; Driver, D. A.; Berg, R. H.; Kim, S. K.; Norden, B.; Nielsen, P. E. *Nature* **1993**, *365*, 566−568.

(36) Murphree, L. J.; Marshall, M. A.; Rieger, J. M.; MacDonald, T. L.; Linden, J. *Mol. Pharmacol.* **2002**, *61*, 455−462.

(37) Jacobson, K. A.; Ukena, D.; Kirk, K. L.; Daly, J. W. *Proc. Natl. Acad. Sci. U.S.A.* **1986**, *83*, 4089−4093.

(38) Ukena, D.; Jacobson, K. A.; Kirk, K. L.; Daly, J. W. *FEBS Lett.* **1986**, *199*, 269−274.

(39) Kozma, E.; Kumar, T. S.; Federico, S.; Phan, K.; Balasubramanian, R.; Gao, Z. G.; Paoletta, S.; Moro, S.; Spalluto, G.; Jacobson, K. A. *Biochem. Pharmacol.* **2012**, *83*, 1552−1561.

(40) Lees, W. J.; Spaltenstein, A.; Kingery-Wood, J. E.; Whitesides, G. M. *J. Med. Chem.* **1994**, *37*, 3419−3433.

(41) Liu, W.; Chun, E.; Thompson, A. A.; Chubukov, P.; Xu, F.; Katrich, V.; Han, G. W.; Roth, C. B.; Heitman, L. H.; IJzerman, A. P.; Cherezov, V.; Stevens, R. C. *Science* **2012**, *337*, 232−236.

(42) Thevenin, D.; Lazarova, T.; Roberts, M. F.; Robinson, C. R. *Protein Sci.* **2005**, *14*, 2177−2186.

(43) He, W.; Crawford, M. J.; Rapireddy, S.; Madrid, M.; Gil, R. R.; Ly, D. H.; Achim, C. *Mol. BioSyst.* **2010**, *6*, 1619−1629.

(44) Autiero, I.; Saviano, M.; Langella, E. *Phys. Chem. Chem. Phys.* **2014**, *16*, 1868−1874.

(45) Canals, M.; Burgueno, J.; Marcellino, D.; Cabello, N.; Canela, E. I.; Mallol, J.; Agnati, L.; Ferre, S.; Bouvier, M.; Fuxe, K.; Ciruela, F.; Lluis, C.; Franco, R. *J. Neurochem.* **2004**, *88*, 726−734.

(46) Fanelli, F.; Felline, A. *Biochim. Biophys. Acta* **2011**, *1808*, 1256−1266.

(47) Huang, J.; Chen, S.; Zhang, J. J.; Huang, X. Y. *Nat. Struct. Mol. Biol.* **2013**, *20*, 419−425.

(48) Manglik, A.; Kruse, A. C.; Kobilka, T. S.; Thian, F. S.; Mathiesen, J. M.; Sunahara, R. K.; Pardo, L.; Weis, W. I.; Kobilka, B. K.; Granier, S. *Nature* **2012**, *485*, 321−326.